Nuclear Science and Techniques (2024) 35:183
https://doi.org/10.1007/s41365-024-01552-9

Moments of inertia of triaxial nuclei in covariant density functional theory

Yu-Meng Wang[1] · **Qi-Bo Chen**[1]

Received: 18 April 2024 / Revised: 17 June 2024 / Accepted: 21 June 2024 / Published online: 28 September 2024

Abstract

The covariant density functional theory (CDFT) and five-dimensional collective Hamiltonian (5DCH) are used to analyze the experimental deformation parameters and moments of inertia (MoIs) of 12 triaxial nuclei as extracted by Allmond and Wood [J. M. Allmond and J. L. Wood, Phys. Lett. B 767, 226 (2017)]. We find that the CDFT MoIs are generally smaller than the experimental values but exhibit qualitative consistency with the irrotational flow and experimental data for the relative MoIs, indicating that the intermediate axis exhibites the largest MoI. Additionally, it is found that the pairing interaction collapse could result in nuclei behaving as a rigid-body flow, as exhibited in the $^{186-192}$Os case. Furthermore, by incorporating enhanced CDFT MoIs (factor of $f \approx 1.55$) into the 5DCH, the experimental low-lying energy spectra and deformation parameters are reproduced successfully. Compared with both CDFT and the triaxial rotor model, the 5DCH demonstrates superior agreement with the experimental deformation parameters and low-lying energy spectra, respectively, emphasizing the importance of considering shape fluctuations.

Keywords Moment of inertia · Trixial nucleus · Covariant density functional theory · Five-dimensional collective Hamiltonian · Low-lying energy spectrum

1 Introduction

The moment of inertia (MoI) is crucial for studying the rotational behavior of nuclei [1–6]. For example, the observation of an abrupt MoI change in a rotational band led to the discovery of the "backbending" phenomenon [7], which has triggered a revolution in the study of the structure of atomic nuclei, which is still currently on-going. Therefore, accurate MoI prediction is a major goal in rotational theory. The MoI has been extensively studied in axially symmetric nuclei. However, our understanding of this phenomenon in triaxially deformed nuclei is relatively limited. A triaxial shape is associated with intriguing phenomena such as the γ band [2], signature inversion [8], anomalous signature splitting [9], wobbling motion [2], and chiral rotation [10]. Among these, wobbling motion and chiral rotation serve as direct evidence of a stable triaxial shape.

Phenomenological MoI models in triaxial nuclei can be categorized into two ideal types: rigid-body and irrotational flow MoIs [1–5]. Rigid-body MoIs consider the nucleus to rotate as a single entity. Consequently, the MoI is calculated by summing the products of each infinitesimal mass element and the square of their distance from the axis of rotation, which depends on deformation parameters (β, γ) as [1–5]

$$\mathcal{J}_{\mathrm{rig},k} = B_{\mathrm{rig}}\left[1 - \sqrt{\frac{5}{4\pi}}\beta\cos\left(\gamma - k\frac{2\pi}{3}\right)\right]. \tag{1}$$

Here, $B_{\mathrm{rig}} = \frac{2}{5}MR^2 = 0.0138 \times A^{5/3}\ \hbar^2/\mathrm{MeV}$ represents the rigid-body inertia parameter. However, experimental MoIs are generally much smaller than rigid-body MoIs [1–5].

Conversely, irrotational-flow MoIs assume that the nucleus behaves like an irrotational liquid, that is, there is an absence of vorticity for the largest possible area in the central sphere. Therefore, only nucleons located outside

This work was supported by the National Natural Science Foundation of China (No. 12205103).

✉ Qi-Bo Chen
qbchen@phy.ecnu.edu.cn

1 Department of Physics, East China Normal University, Shanghai 200241, China

the central sphere contribute to the MoI. Correspondingly, irrotational-flow MoIs are given as [1–5]

$$\mathcal{J}_{\mathrm{irr},k} = 4B_{\mathrm{irr}}\beta^2 \sin^2\left(\gamma - k\frac{2\pi}{3}\right), \tag{2}$$

where $B_{\mathrm{irr}} = \frac{3}{8\pi}MR^2 = 0.00412 \times A^{5/3}\ \hbar^2/\mathrm{MeV}$ represents the irrotational flow inertia parameter.

There are key differences between these two MoI types. First, $\mathcal{J}_{\mathrm{irr},k}$ becomes zero along the symmetric axis, whereas $\mathcal{J}_{\mathrm{rig},k}$ does not. Second, $\mathcal{J}_{\mathrm{irr},k}$ indicates that the intermediate axis exhibits the largest MoI, whereas $\mathcal{J}_{\mathrm{rig},k}$ suggests that the short axis exhibits the largest MoI. This leads to the observation that $\mathcal{J}_{\mathrm{irr},k}$ can induce a phenomenon known as transverse wobbling motion [11] and chiral rotation [10], while $\mathcal{J}_{\mathrm{rig},k}$ lacks this capability. Finally, $\mathcal{J}_{\mathrm{irr},k}$ strongly depends on the deformation parameter β^2, whereas $\mathcal{J}_{\mathrm{rig},k}$ is less sensitive to deformation and is roughly proportional to β. Overall, for a given deformation β, $\mathcal{J}_{\mathrm{rig},k}$ generally exceeds $\mathcal{J}_{\mathrm{irr},k}$, indicating a significant difference in magnitude between these two MoIs.

In 2017, Allmond and Wood [12] analyzed a dozen triaxially deformed nuclei using experimental data for 2^+ state energies and the electric quadrupole matrix elements. They compared the extracted deformation parameters and empirical MoIs for all three principal axes with predictions from rigid and irrotational flow models. Their results showed that the absolute MoIs were between the values expected from the two models. However, the relative MoIs exhibited qualitative consistency with the $\beta^2 \sin^2\gamma$ -dependence for the irrotational-flow MoI. This was the first report of empirical MoIs for all three principal axes in triaxially deformed nuclei. Subsequently, Schuck and Urban [13] showed that these empirical MoIs can be explained via semiclassical cranked Hartree-Fock-Bogoliubov (HFB) [14, 15] calculations, which superimpose the rigid and irrotational flow contributions. The agreement between theory and experiment suggests the macroscopic behavior of nuclei. However, this approach neglected the shell effects. Hence, it is important to investigate MoIs using a fully microscopic approach considering these effects. Moreover, it has been recognized that certain studied nuclei exhibit significant β and γ fluctuations, and could deviate from the extracted average values [12]. Therefore, it is imperative to comprehensively investigate these fluctuations and their implication.

Microscopically, the Inglis formula [1, 3, 4, 6, 16] can be used to study MoIs by constraining the wave functions to rotate at a constant angular velocity, $\boldsymbol{\omega}$. However, neglecting pairing correlations in this formula yields MoI values close to those of rigid-body predictions. For improved accuracy, the Inglis-Belyaev (IB) formula considers pairing correlations within the BCS formulation [1, 3, 4, 6, 17]

$$\mathcal{J}_k = \sum_{ij} \frac{(u_i v_j - v_i u_j)^2}{E_i + E_j} \left| \langle i | \hat{J}_k | j \rangle \right|^2, \quad k = 1, 2, 3, \tag{3}$$

where E_i, v_i, and $|i\rangle$ denote the quasi-particle energies, occupation probabilities, and single-nucleon wave functions, respectively. The summation runs over the proton and neutron quasi-particle states. It is worth noting that the IB formula incorporates the effects of nucleon pairing and shell structure on MoIs.

In this work, we will employ the state-of-the-art covariant density functional theory (CDFT) as a microscopic approach for studying MoIs. The CDFT is a comprehensive and reliable tool for investigating the ground-state properties of spherical and deformed nuclei throughout a nuclide chart [18–25]. Within the mean-field approximation, MoIs can be calculated in a fully microscopic and self-consistent manner using the IB formula [26, 27]. However, to accurately describe the low-lying energy spectra, we must go beyond the static mean-field approximation. Accordingly, we will adopt a five-dimensional collective Hamiltonian (5DCH) approach [2, 3, 5, 23, 28–36], that considers five quadrupole dynamic degrees of freedom: deformation parameters (β, γ) and nucleus orientation angles $\boldsymbol{\Omega}(\phi, \theta, \psi)$. Furthermore, the collective parameters in 5DCH, including the MoIs, are determined via CDFT calculations, that is, using 5DCH-CDFT [23, 26, 27, 33, 36]. The 5DCH-CDFT has achieved great success in studying various nuclear collective properties such as phase transitions [27, 37–40], shape evolution [26, 41–56], tidal waves [57], and the nuclear landscape considering beyond-mean-field dynamic correlation energies [58, 59]. For a comprehensive review, see Refs. [23, 33, 36].

In this paper, we will investigate the deformation parameters and MoIs for the reported 12 triaxially deformed nuclei using 5DCH-CDFT. The calculated deformation parameters and MoIs will be compared with existing experimental data and rigid and irrotational-flow MoIs. Additionally, we will study the low-lying energy spectra of these nuclei to validate the CDFT MoI predictions.

2 Numerical details

The detailed theoretical framework for 5DCH-CDFT can be found in Refs. [23, 26, 27, 33, 36]. For the CDFT calculations, we employ the point-coupling energy density functional PC-PK1 in the particle-hole channel and the density-independent δ force in the particle-particle channel, as described in [60]. The δ-force strength parameter is set to 349.5 MeV fm^3 (330.0 MeV fm^3) for neutron (proton) pairing, which is calibrated by fitting an empirical neutron (proton) pairing gap [60]. To solve the equation of motion for nucleons, we expand the Dirac spinors in a set of three-dimensional harmonic oscillator basis functions in Cartesian coordinates with 14 major shells. This provides an accurate representation of the nucleon spatial distribution within the nucleus. To determine the collective parameters on the (β, γ)-plane for the 5DCH, we perform constrained triaxial CDFT calculations in the $\beta \in [0.0, 0.8]$ and $\gamma \in [0°, 60°]$ regions, with a step size of $\Delta\beta = 0.05$ and $\Delta\gamma = 6°$, respectively.

3 Results and discussion

3.1 Potential energy surfaces

Figure 1 shows the potential energy surfaces (PESs) in the (β, γ)-plane for the 12 triaxial nuclei obtained from the CDFT calculations with an effective interaction PC-PK1 [60]. For comparison, the experimental deformation parameters from previous studies [12] are also included for comparison. For ^{110}Ru, a triaxial deformation of $(\beta = 0.26, \gamma = 40°)$ is observed. The predicted β and γ values are slightly smaller and larger than the experimental values of 0.310(11) and 29.0°(4.8°) [12], respectively. The PES of this nucleus is relatively flat in the β- and γ-directions toward the oblate side. By contrast, for ^{150}Nd, ^{156}Gd, ^{166,168}Er, ^{172}Yb, and ^{182,184}W, the minimum is located at $\gamma = 0°$, i.e., it exhibits a prolate shape, which disagrees with the triaxial deformation indicated by the experimental data. Around the calculated minimum, the curve is relatively flat along the γ-direction toward the experimental deformation parameters (≈ 0.5 MeV). Nevertheless, these findings underscore the limitations of the mean-field approximation used in the CDFT calculations and suggest that the additional refinements, such as those for the fluctuation effects, are necessary to improve the predictions for these nuclei (c.f. Fig. 10). For $^{186-192}$Os, the CDFT calculations show good agreement with the experimental data for ground-state deformation parameters. The minima γ values range between 20° and 30°, indicating the importance of triaxial deformation in these nuclei.

3.2 Moments of inertia

Using the obtained single-nucleon wave functions, energies, and occupation factors generated from the constrained self-consistent CDFT solutions, we calculate the MoIs using the IB formula for all three principal axes [23, 26, 27, 33, 36]. The calculated MoIs, denoted as $\mathcal{J}_{\mathrm{CDFT},k}$, are plotted as a function of $\beta^2 \sin^2(\gamma - 2k\pi/3)$ and γ, as shown in Fig. 2. For comparison, the experimental values, denoted as $\mathcal{J}_{\mathrm{Exp},k}$ [12], are also plotted. As shown in Fig. 1, the predicted deformation parameters obtained via CDFT are not ideally identical to the experimental parameters. This can lead to ambiguity when comparing the CDFT-predicted and experimental MoIs. To address this issue, the deformation parameters used in the CDFT calculations are constrained to be the same as the experimental parameters [12]. Finally, the obtained $\mathcal{J}_{\mathrm{CDFT},k}$ are compared with $\mathcal{J}_{\mathrm{rig},k}$ (1) and $\mathcal{J}_{\mathrm{irr},k}$ (2).

Figure 2 shows that both the experimental and CDFT MoIs fall between the expectations of rigid and irrotational motions. This suggests that the flow structures within realistic nuclei are neither purely irrotational nor rigid. The $\mathcal{J}_{\mathrm{Exp},k}$ values are found to be 6.3, 7.4, and 10.0 times larger than the $\mathcal{J}_{\mathrm{irr},k}$ values for the intermediate (m, 1-axis), short (s, 2-axis), and long (l, 3-axis) axes, respectively. Correspondingly, the ratios $\mathcal{J}_{\mathrm{CDFT},k}$ are smaller at 4.5, 5.8, and 10.0. This underestimation is due to the use of the IB formula without considering the Thouless-Valatin dynamic rearrangement [61–64]. Therefore, the order of MoIs for the different models can be expressed as: $\mathcal{J}_{\mathrm{irr},k} < \mathcal{J}_{\mathrm{CDFT},k} < \mathcal{J}_{\mathrm{Exp},k} < \mathcal{J}_{\mathrm{rig},k}$.

To investigate whether $\mathcal{J}_{\mathrm{CDFT},k}$ follows the properties of $\mathcal{J}_{\mathrm{irr},k}$, we examine their relative MoIs as functions of γ, as shown in Fig. 3, and compare them with the experimental data [12] for all three principal axes. The scale used in Fig. 3 is normalized to $\mathcal{J}_1$, which represents the MoI of the m-axis. We find that the relative $\mathcal{J}_{\mathrm{CDFT},k}$ are also qualitatively consistent with $\mathcal{J}_{\mathrm{irr},k}$ and in agreement with $\mathcal{J}_{\mathrm{Exp},k}$. This agreement confirms the validity of the CDFT approach for describing the triaxially deformed nuclei. It is worth noting that the MoIs calculated using the cranking model based on the modified oscillator potential exhibit the same behavior as $\mathcal{J}_{\mathrm{irr},k}$ [65]. These results demonstrate the importance of considering $\mathcal{J}_{\mathrm{irr},k}$ to understand the collective rotational behavior of triaxially deformed nuclei. For example, the m axis exhibits the largest MoI, which leads to the appearance of transverse wobbling in the low-spin region [11, 65, 66] as well as chiral rotation when the nucleus possesses a particle-hole configuration [10, 67–70].

3.3 Moments of inertia in ^{190}Os

Notably, as shown in Fig. 3, the calculated relative MoIs for $^{186-192}$Os along the l axis are overestimated compared with the experimental values, which contradicts the trend for $\mathcal{J}_{\mathrm{irr},k}$. To investigate this discrepancy, we further analyze the ^{190}Os case. Using the CDFT, we calculate the MoIs as a function of γ for fixed values of $\beta = 0.1, 0.2, 0.3$, and 0.5. Additionally, the individual contributions from neutrons and protons to the MoIs are also analyzed, as shown in Fig. 4. As β increases, the degree of asymmetry becomes more pronounced. The relative MoIs along the s axis remain consistent with the irrotational flow, and significant deviations occur at $\beta = 0.1$ and 0.2. Intriguingly, for the l axis MoI, a peculiar phenomenon is observed. At $\gamma = 0°$, the relative MoIs for $\beta = 0.1$ and 0.2 do not vanish, which exceeds the expectation for a prolate shape.

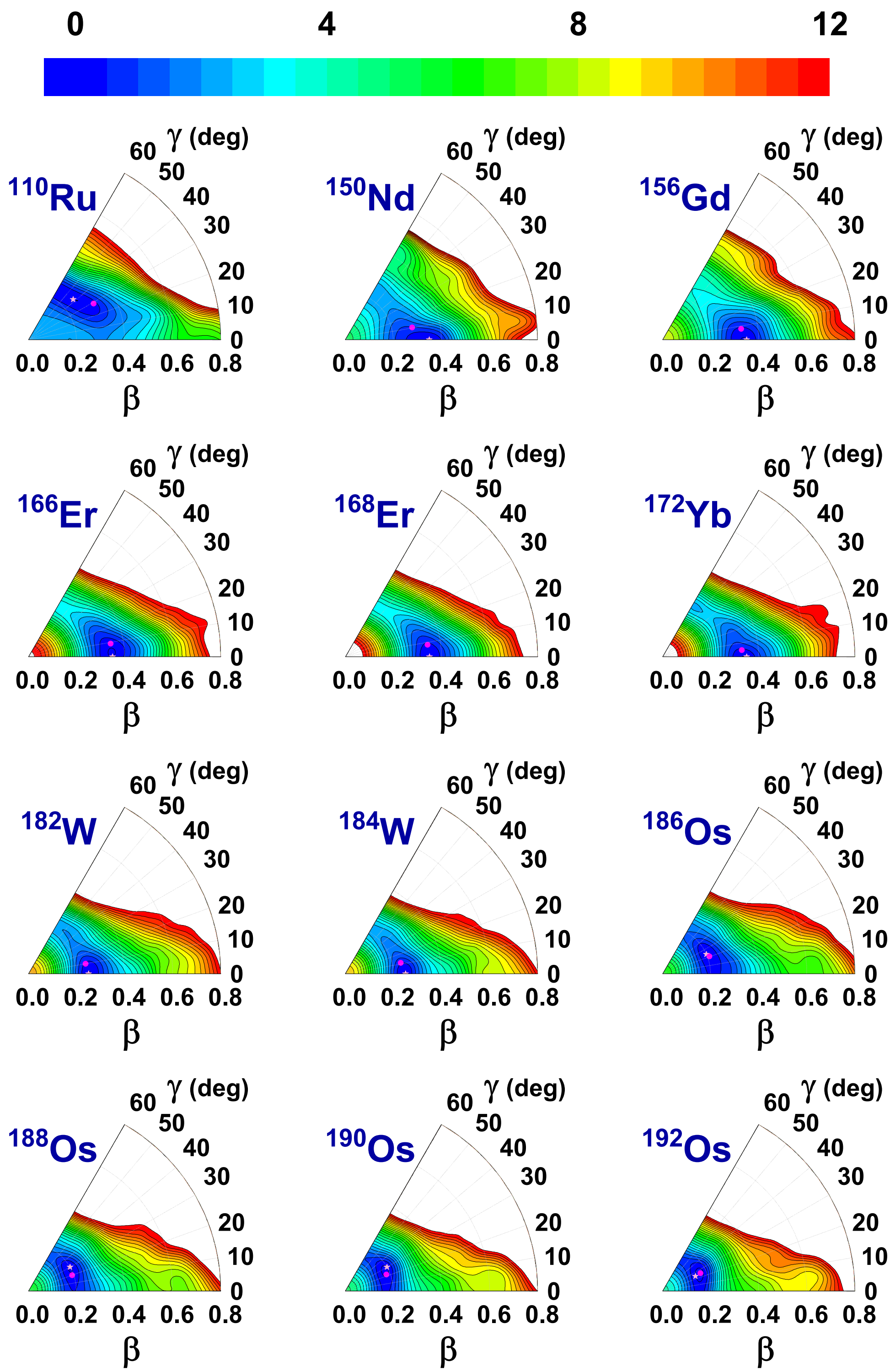

Fig. 1 (Color online) Potential energy surfaces in the (β, γ) -plane for 12 nuclei calculated via CDFT. All energies are normalized with respect to the minimum (stars). The contour lines are spaced at 0.5 MeV intervals. Experimental deformation parameters from the literature [12] are included (dots) for comparison

Additionally, the contributions of protons and neutrons are substantially different at $\beta = 0.2$, with the proton contribution being significantly larger than that of neutrons. However, when $\beta = 0.3$ and 0.5, the l axis relative MoI returns to zero.

To investigate the potential influence of β deformation on the MoI behavior with respect to γ for isotope ^{190}Os, we calculate the MoIs for both the m and l axes as a function of β, while maintaining γ fixed at 0Å, as shown in Fig. 4. It is worth noting that when γ is set to 0Å, $\mathcal{J}_m$ is equal to $\mathcal{J}_s$. Additionally, we plot the individual contributions of

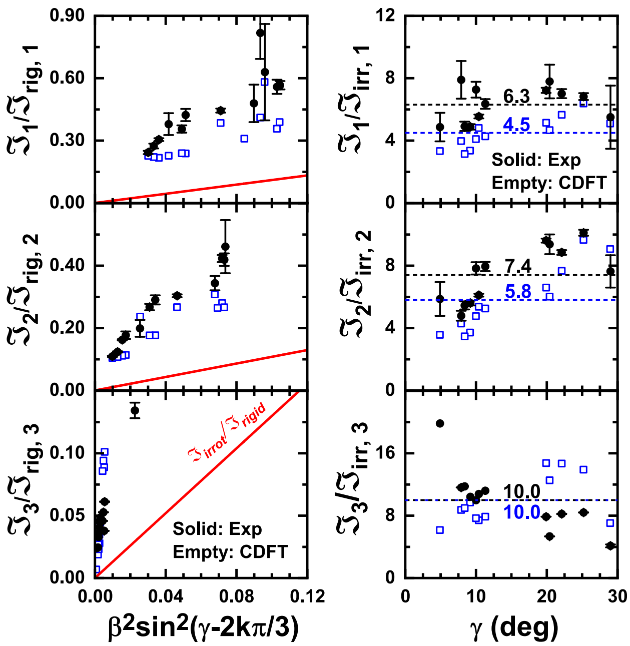

Fig. 2 (Color online) Left: CDFT, experimental, and irrotational-flow MoIs relative to the rigid-body value as functions of $\beta^2 \sin^2(\gamma - 2k\pi/3)$ for the 1-, 2-, and 3-axes, corresponding to the m, s, and l axes, respectively. Right: CDFT and experimental MoIs relative to the irrotational flow value as functions of γ for the m, s, and l axes. The dashed lines represent the average ratio of the 12 nuclei

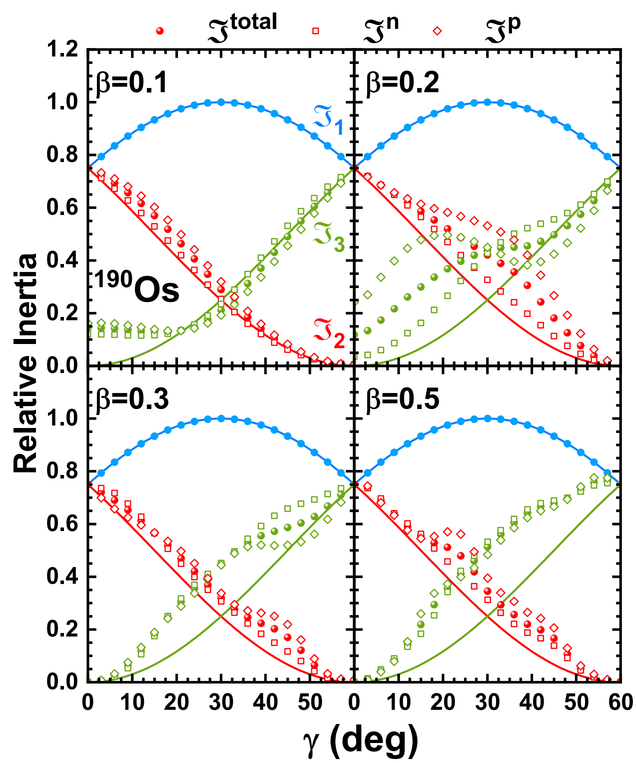

Fig. 4 (Color online) Same as Fig. 3, but for [190] Os at $\beta = 0.1$, 0.2, 0.3, and 0.5

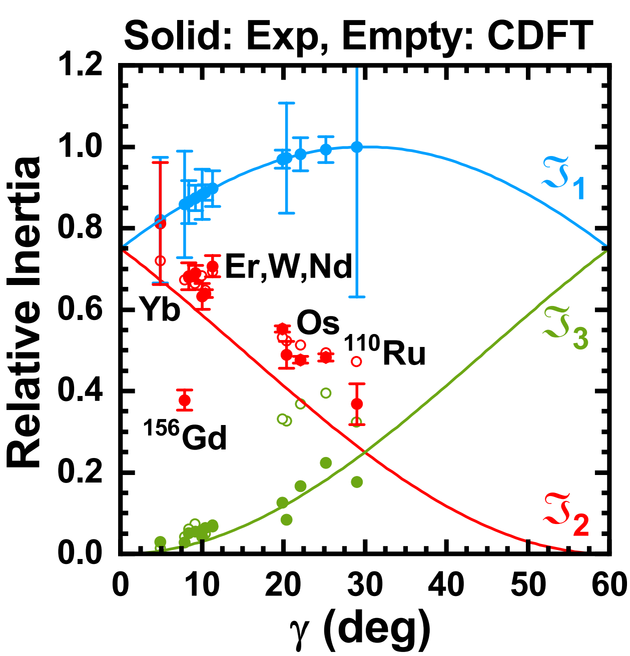

Fig. 3 (Color online) Relative MoIs for all three principal axes as functions of γ. The CDFT and experimental values are normalized to the irrotational values using the 1-axis (m axis) as a reference

neutrons and protons to the MoIs, as shown in Fig. 5. To further analyze the results, we compare them with those obtained for ^{168}Er, which exhibit good agreement with $\mathcal{J}_{\mathrm{irr},k}$, as shown in Fig. 3. Figure 5 shows the $\mathcal{J}_m$ and $\mathcal{J}_l$ behavior for ^{168}Er, revealing an increasing trend in $\mathcal{J}_m$ as the deformation β increases, which is expected given that the degree of the asymmetry increases. Conversely, $\mathcal{J}_l$ aligns with the anticipated behavior for a prolate shape, namely, it approaches zero. However, for ^{190}Os, noticeable deviations are observed, particularly for $\mathcal{J}_l$ values that do not vanish within a range of β values between 0.08–0.22 (as indicated by the vertical lines in the figure).

As mentioned previously, the MoIs in the CDFT are calculated using the IB formula, which are determined from the quasi-particle energy of the quasi-particle states in the denominator and matrix elements of the angular momentum in the quasi-particle states in the numerator. In particular, the single-particle energy levels near the Fermi surface play a decisive role in determining the MoIs. Thus, to elucidate the reason behind the non-vanishing $\mathcal{J}_l$ values for ^{190}Os shown in Fig. 5, we investigate the corresponding single-particle energy levels of protons and neutrons for ^{190}Os as a function of β. We compare these results with those for ^{168}Er, which serve as a reference, as shown in Fig. 6. Upon examining the single-particle energy levels for protons in ^{190}Os, we observe that the energy level density near the Fermi surface

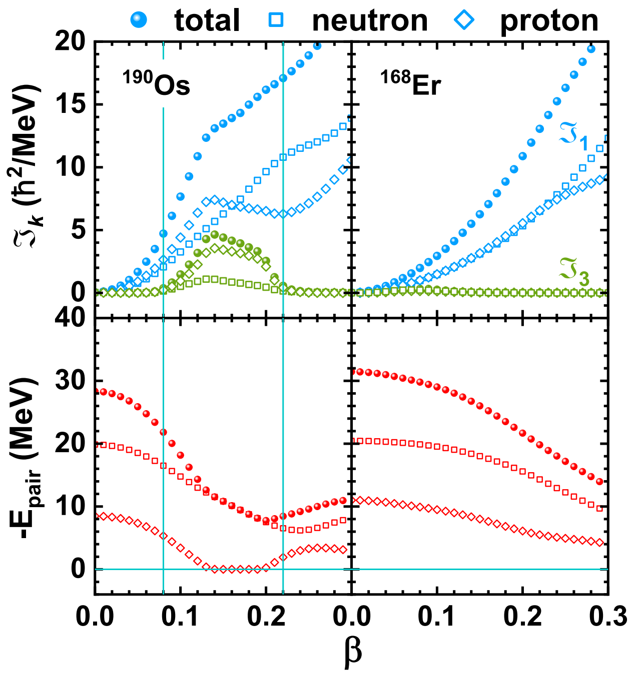

Fig. 5 (Color online) Calculated MoIs (upper) and pairing energy (lower) of the total, neutron, and proton as functions of β for ^{168} Er (left) and ^{190} Os (right). The vertical lines label the region of nonzero $\mathcal{J}_l$ for ^{190} Os, while the horizontal lines label the vanishing of pairing energy

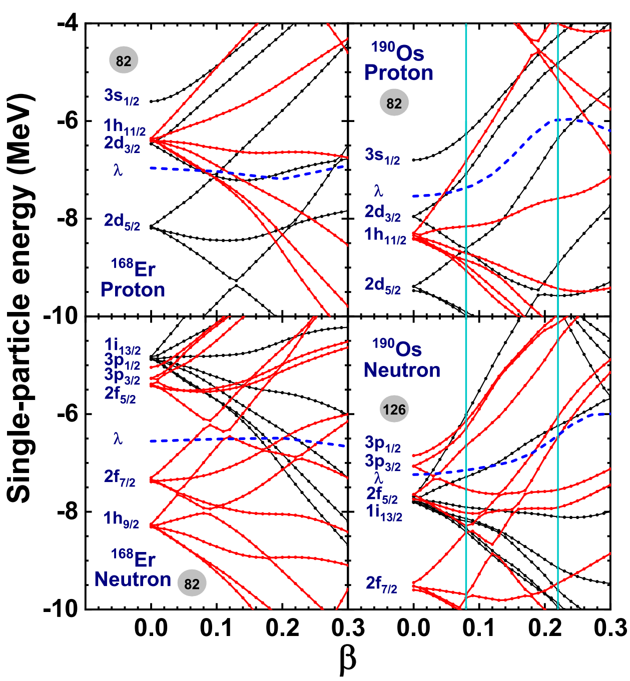

Fig. 6 (Color online) Partial proton (upper) and neutron (lower) single-particle energy levels as functions of β at $\gamma = 0°$ for ^{168} Er (left) and ^{190} Os (right). The dashed line denotes the Fermi surface

in the region of $0.08 \leq \beta \leq 0.22$ is much smaller than that of the other, which may indicate a decrease in the pairing interaction. Indeed, a quantitative study of microscopic nuclear level densities based on CDFT, as in Refs. [72, 73], would be interesting.

To study the effect of pairing interactions, we plot the pairing energy, as shown in the lower panels of Fig. 5. It can be clearly seen that in the region of $0.08 \leq \beta \leq 0.22$, the proton-pairing energy tends to vanish, indicating the collapse of the proton pairing interaction. Consequently, the MoI of the l axis of proton does not disappear and behaves like a rigid MoI, as previously mentioned. Beyond this region, the pairing energy is a finite value and the proton $\mathcal{J}_l$ becomes zero. However, no pairing collapse occurred for ^{168} Er, and $\mathcal{J}_l$ is zero. It is noted that in the selected PC-PK1 interaction [60], the pairing strengths are fixed at specific values: $G_{\rm n} = 349.5$ MeV fm^3 for neutrons and $G_{\rm p} = 330.0$ MeV fm^3 for protons. To further explore the potential impact of varying pairing strengths on the final outcome, we analyze the calculated MoIs and pairing energies of the total neutrons and protons as a function of β for the nucleus ^{190} Os, as shown in Fig. 7. Specifically, we maintain $G_{\rm n}$ at 349.5 MeV fm^3 while adjusting $G_{\rm p}$ from 0.0 to 165.0 (half of the original $G_{\rm p}$ strength) and 660.0 MeV fm^3 (twice the original $G_{\rm p}$ strength). The observations reveal that when $G_{\rm p}$ is reduced or eliminated, the proton-pairing energy is significantly diminished. Consequently, there is a corresponding increase in the proton moment of inertia $\mathcal{J}_l$. In comparison with the case of the original $G_{\rm p}$ strength, the proton pairing collapse occurs in a larger β region. When $G_{\rm p}$ is enhanced, the proton-pairing energy increases dramatically. This results in a vanishing proton $\mathcal{J}_l$. Hence, this

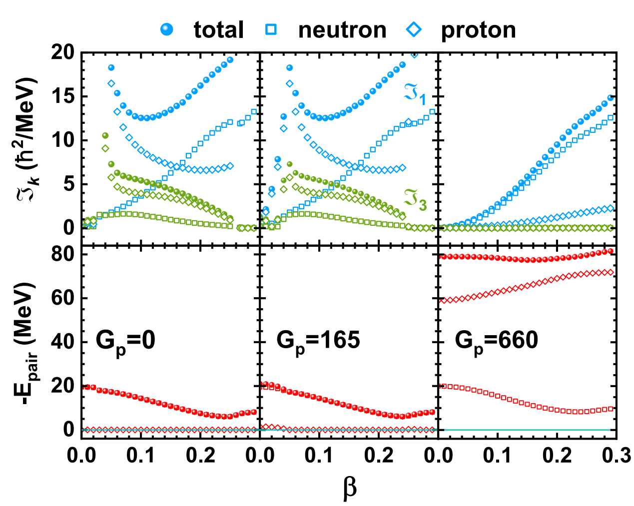

Fig. 7 (Color online) Calculated MoIs (upper) and pairing energy (lower) of the total, neutron, and proton as functions of β for ^{190} Os with $G_{\rm p} = 0.0$ (left), 165.0 (middle), and 660.0 MeV fm^3 (right)

indicates that rigid flow is a consequence of the collapse of the pairing interaction from irrotational flow. However, it should be noted that the underlying mechanism behind this phenomenon is still not fully understood. Additionally, we note that the pairing energy collapse is attributed to the fact that the present pairing correlations are treated in the BCS approximation without particle number projection. To avoid this problem, restoring particle number symmetry is necessary [3]. However, this is beyond the scope of the present study. Nevertheless, the importance of pairing correlations on the nuclear structure and also, for example, on the fragment mass distribution [74] and β-decay half-lives [75] are already well known.

3.4 Low-lying energy spectra

To further assess the predictive power of CDFT for the MoIs, we investigate the energy spectra of the ground-state, β, and γ bands in the 12 triaxial nuclei using 5DCH based on CDFT inputs. As shown in Fig. 2, the calculated CDFT MoI values significantly underestimate the empirical results owing to neglecting the Thouless-Valatin corrections that are largely independent of deformation [62–64]. Therefore, we enhance the CDFT MoI values using a constant factor f ($\approx$ 1.55) to fit the experimental 2_1^+ state energy. The results are presented in Fig. 8 along with the available experimental data obtained from the National Nuclear Data Center (NNDC) [71]. Note that the collective potentials in the 5DCH include the zero-point energy (ZPE) corrections originating from vibrational and rotational kinetic energy [26]. We label this enhanced factor f used in the calculations for each subfigure to provide clarity. As shown in Fig. 8, the 5DCH energy spectra and the corresponding experimental data for the 12 triaxial nuclei are generally in good agreement. This agreement not only validates the effectiveness of the 5DCH but also provides further support for the overall validity of the CDFT approach for describing the nuclear dynamics of triaxially deformed nuclei.

However, the 5DCH predictions may differ from the experimental observations in certain cases. Specifically, for ^{110}Ru, the theoretical γ band energies are slightly higher than the experimental values. For ^{150}Nd, ^{156}Gd, and ^{168}Er, while the γ band is reproduced, the β-band energy is overestimated, indicating that the mass parameter along the β -direction is underestimated. For ^{172}Yb, the energy crossings between the β and γ bands are less evident in the calculations. For ^{182,184}W and ^{186}Os, the β-band slope is overestimated, indicating that the MoI in the β band is too small. Therefore, there is room for improvement in the theoretical models used in this study. For instance, the inclusion of dynamic pairing vibrations can improve the description of the 0^+ state of the β band [76]. A more streamlined approach involves considering the enhancement of the mass parameters by a scaling factor, which is denoted by f'. For further

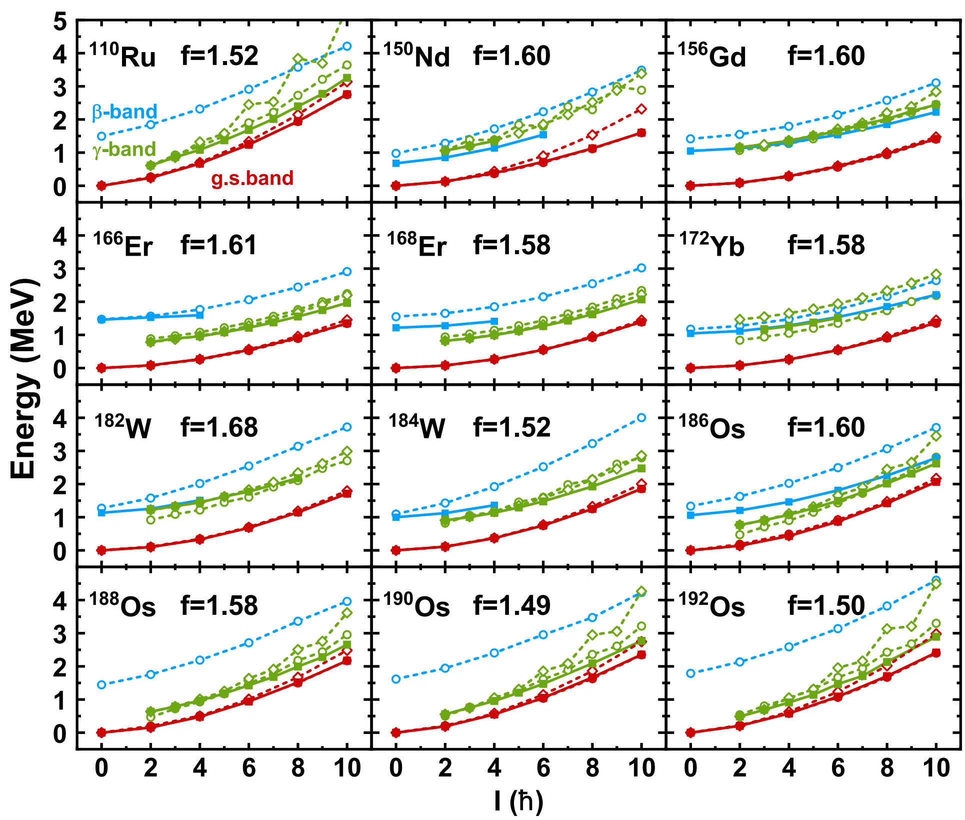

Fig. 8 (Color online) Energy spectra of the ground-state, β, and γ bands for the 12 nuclei calculated via the 5DCH (open circles) in comparison with those obtained from TRM calculations (open diamonds) and available experimental data (solid symbols) from NNDC [71]. The f value represents the enhanced factor for CDFT MoIs used in the 5DCH

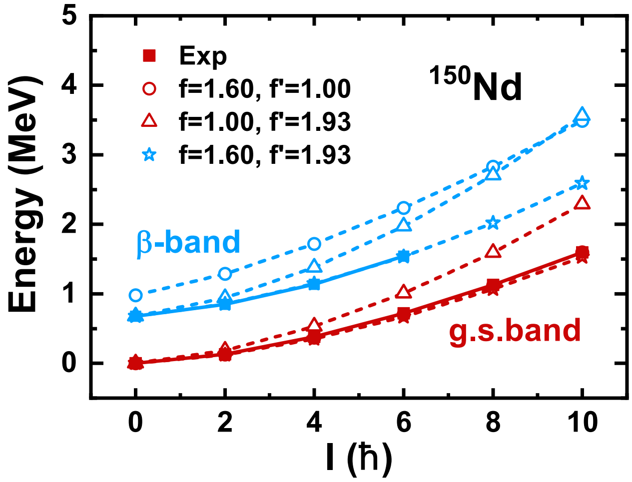

Fig. 9 (Color online) Energy spectra for the ground-state and β bands in ^{150} Nd calculated via 5DCH (open symbols) compared with available experimental data (solid symbols) from NNDC [71]. The f and f' values respectively represent the enhanced factors for the CDFT MoIs and mass parameter $B_{\beta\beta}$ used in the 5DCH

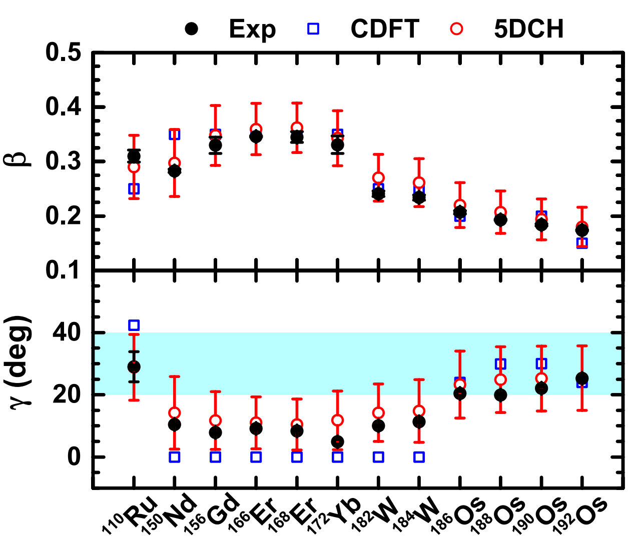

Fig. 10 (Color online) Deformation parameters $\bar{\beta}$ (upper) and $\bar{\gamma}$ (lower) of the 0_1^+ state in 5DCH (open circles) compared with the ground state deformation parameters in CDFT (open squares) and experimental data (solid circles) for 12 nuclei [12]. In the 5DCH results, the $\Delta\beta$ and $\Delta\gamma$ fluctuations are depicted as positive and negative error bars for $\bar{\beta}$ and $\bar{\gamma}$, respectively. The light-blue band represents the region of remarkable triaxial deformation

investigation, we select the nuclide ^{150} Nd as a representative example. Figure 9 shows the obtained energy spectra of the ground-state and β bands in ^{150} Nd using the 5DCH method, juxtaposed with pertinent experimental data from NNDC [71]. The analysis results reveal that exclusively enhancing the MoIs leads to an overestimation of the excitation energy within the β band. Similarly, enhancing only the mass parameter along the β-direction, denoted as $B_{\beta\beta}$, leads to an overestimation of the slopes exhibited by the ground-state and β bands. Notably, when both the MoIs and $B_{\beta\beta}$ are enhanced concurrently, the computed energy spectra for both the ground-state and β bands align favorably with the experimental observations.

To examine the fluctuation effects in the 5DCH, we perform rigid triaxial rotor model (TRM) [2] calculations using the experimental MoIs along the three principal axes [12] as inputs. The TRM does not consider the β degree of freedom and cannot predict the β band. Therefore, Fig. 8 shows the TRM results for the ground-state and γ bands. The TRM successfully reproduces the ground-state band energies for ^{156} Gd, ^{166,168} Er, ^{172} Yb, ^{182,184} W, and ^{186} Os. It also describes the γ-band behavior for these nuclei. However, this method overestimates the ground-state band energies in the high-spin region for ^{110} Ru^{150} Nd, and $^{188\text{-}192}$ Os, resulting in poorly described γ bands with higher energies and a more pronounced staggering behavior, that is, indicating the γ deformation degrees of freedom is estimated to be too rigid [7]. In contrast, the 5DCH calculations show better agreement in these cases, highlighting the importance of considering the fluctuations in the deformation degree of freedom.

Using the 5DCH wave functions, we calculate the deformation expectation $\bar{\beta}$ and $\bar{\gamma}$ and their fluctuations $\Delta\beta$ and $\Delta\gamma$ [38], and compare these values for the 0_1^+ state with those obtained from the CDFT ground-state calculations and the experimental data [12], as shown in Fig. 10. While the CDFT ground-state deformation parameters deviate from the experimental values for some nuclei, the 5DCH accurately reproduces the experimental data. In particular, the nuclei predicted to have an axial shape in the CDFT calculations exhibit triaxiality in the 5DCH, emphasizing the significance of considering the fluctuations in the deformation degree of freedom. Additionally, we find that the $\bar{\beta}$ value of the 5DCH is similar to that of CDFT for all nuclei except for ^{110} Ru and ^{150} Nd, suggesting a relatively small fluctuation in the β direction in these nuclei. However, only ^{110} Ru and $^{186\text{-}192}$ Os exhibit notable triaxial deformation parameters ($20° \leq \gamma \leq 40°$), as indicated by the light-blue band in Fig. 10. Additionally, all nuclei display significant fluctuations in triaxial deformation ($\Delta\gamma \approx 10°$), which indicates a certain degree of γ softness. Therefore, the occurrence of rigid triaxially deformed ground states remains uncommon.

Furthermore, utilizing the obtained 5DCH wavefunctions, we calculate the in-band $E2$ transition probabilities $B(E2)$ and compare these calculations with the available experimental data for Os isotopes $^{186\text{-}192}$ Os [71], which exhibit notable triaxiality (c.f. Fig. 10), as shown in Fig. 11. Note that $E2$ transition results for additional nuclei can be referenced from Refs. [27, 40, 52, 54]. Despite a slight overestimation by the 5DCH approach compared with the

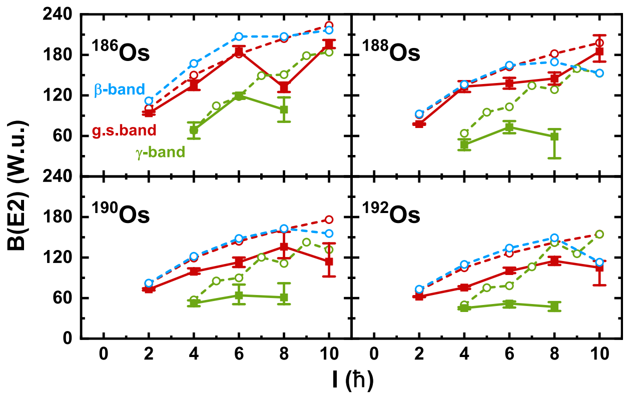

Fig. 11 (Color online) Calculated in-band $B(E2)$ transition probabilities of the ground-state, γ, and β bands for $^{186-192}$ Os in the 5DCH compared with the available data [71]

experimental data, the agreement is reasonable. This is attributed to the significant advantage of the 5DCH-CDFT methodology: transition probabilities are computed within the entire configuration space, thus obviating the need for effective charges. This underscores the robustness of the 5DCH approach for transition probability calculations.

4 Summary

In summary, the MoIs for 12 triaxially deformed nuclei are investigated using the CDFT and 5DCH frameworks. The calculated deformation parameters, MoIs, and low-lying energy spectra are compared with available experimental data.

The results reveal that the absolute MoIs derived via CDFT are generally smaller than the experimental values, but exhibit qualitative consistency with irrotational flow and experimental data. Therefore, the m axis exhibits the largest MoI and it is more appropriate to use MoIs derived from irrotational flow instead of a rigid body when studying rotational behavior. However, it is found that the calculated relative MoIs for $^{186-192}$ Os deviated from the trend expected for irrotational flow. This discrepancy can be attributed to the collapse of pairing interaction, which leads to the nuclei behaving like a rigid-body flow. However, the underlying mechanism for this phenomenon remains unclear.

The 5DCH calculations incorporate an enhanced factor (a factor of $f \approx 1.55$) to address the MoI underestimation by CDFT. Compared with the TRM and CDFT calculations, the 5DCH results agree better with the experimental low-lying energy spectra and deformation parameters. These results emphasize the importance of considering deformation degree of freedom fluctuations. Overall, a rigid triaxially deformed ground state is rare.

Despite these insightful findings, there is still room for improvement in our theoretical models. For example, it was pointed out that enhancing the calculation accuracy for mass parameters can improve the description of the low-lying energy spectra, particularly for the 0^+ state and $E0$ transitions [78]. Extending the scope of work to other novel nuclear collective excitations or unstable nuclei [79–82] is also of interest. By refining these calculations, we could enhance the overall predictive power of the theoretical framework and gain a deeper understanding of the underlying nuclear dynamics.

Acknowledgements The authors would like to thank Professor Zhipan Li for providing the 5DCH numerical code and constructive suggestions. We would also like to thank Professor Tamara Nikšić and Dr. Jian Xiang for their discussions regarding the moment of inertia.

Author Contributions All authors contributed to the study conception and design. Material preparation, data collection and analysis were performed by Yu-Meng Wang and Qi-Bo Chen. The first draft of the manuscript was written by Yu-Meng Wang and all authors commented on previous versions of the manuscript. All authors read and approved the final manuscript.

Data Availability Statement The data that support the findings of this study are openly available in Science Data Bank at https://cstr.cn/31253.11.sciencedb.j00186.00241 and https://doi.org/10.57760/sciencedb.j00186.00241.

Declarations

Conflict of interest The authors declare that they have no Conflict of interest.

References

1. D.J. Rowe, *Nuclear Collective Motion: Models and Theory* (Methuen, London, 1970)
2. A. Bohr, B.R. Mottelson, *Nuclear Structure*, vol. II (Benjamin, New York, 1975)
3. P. Ring, P. Schuck, *The Nuclear Many Body Problem* (Springer Verlag, Berlin, 1980)
4. S.G. Nilsson, I. Ragnarsson, *Shapes and Shells in Nuclear Structure* (Cambridge University Press, Cambridge, 1995)
5. D.J. Rowe, J.L. Wood, *Fundamentals of Nuclear Models: Foundational Models* (World Scientific, Singapore, 2010)
6. Z. Szymanski, *Fast Nuclear Rotation* (Clarendon Press, Oxford, 1983)
7. A. Johnson, H. Ryde, J. Sztarkier, Evidence for a "singularity'' in the nuclear rotational band structure. Phys. Lett. B **34**, 605 (1971). https://doi.org/10.1016/0370-2693(71)90150-X
8. R. Bengtsson, H. Frisk, F.R. May et al., Signature inversion – a fingerprint of triaxiality. Nucl. Phys. A **415**, 189 (1984). https://doi.org/10.1016/0375-9474(84)90620-1
9. I. Hamamoto, H. Sagawa, Triaxial deformation in odd- Z light rare-earth nuclei. Phys. Lett. B **201**, 415 (1988). https://doi.org/10.1016/0370-2693(88)90593-X
10. S. Frauendorf, J. Meng, Tilted rotation of triaxial nuclei. Nucl. Phys. A **617**, 131 (1997). https://doi.org/10.1016/S0375-9474(97)00004-3

11. S. Frauendorf, F. Dönau, Transverse wobbling: a collective mode in odd- A triaxial nuclei. Phys. Rev. C **89**, 014322 (2014). https://doi.org/10.1103/PhysRevC.89.014322
12. J.M. Allmond, J.L. Wood, Empirical moments of inertia of axially asymmetric nuclei. Phys. Lett. B **767**, 226 (2017). https://doi.org/10.1016/j.physletb.2017.01.072
13. P. Schuck, M. Urban, Macroscopic manifestations of rotating triaxial superfluid nuclei. Phys. Rev. C **100**, 031301 (2019). https://doi.org/10.1103/PhysRevC.100.031301
14. M. Farine, P. Schuck, X. Viñas, Moment of inertia of a trapped superfluid gas of atomic fermions. Phys. Rev. A **62**, 013608 (2000). https://doi.org/10.1103/PhysRevA.62.013608
15. M. Urban, P. Schuck, Slow rotation of a superfluid trapped fermi gas. Phys. Rev. A **67**, 033611 (2003). https://doi.org/10.1103/PhysRevA.67.033611
16. D.R. Inglis, Particle derivation of nuclear rotation properties associated with a surface wave. Phys. Rev. **96**, 1059 (1954). https://doi.org/10.1103/PhysRev.96.1059
17. S.T. Belyaev, Concerning the calculation of the nuclear moment of inertia. Nucl. Phys. **24**, 322 (1961). https://doi.org/10.1016/0029-5582(61)90384-4
18. P. Ring, Relativistic mean field theory in finite nuclei. Prog. Part. Nucl. Phys. **37**, 193 (1996). https://doi.org/10.1016/0146-6410(96)00054-3
19. G.A. Lalazissis, P. Ring, D. Vretenar, Extended density functionals in nuclear structure physics. Lecture notes in physics. Springer Berlin, Heidelberg, (2004). https://doi.org/10.1007/b95720
20. D. Vretenar, A.V. Afanasjev, G.A. Lalazissis et al., Relativistic Hartree-Bogoliubov theory: static and dynamic aspects of exotic nuclear structure. Phys. Rep. **409**, 101 (2005). https://doi.org/10.1016/j.physrep.2004.10.001
21. J. Meng, H. Toki, S.G. Zhou et al., Relativistic continuum Hartree Bogoliubov theory for ground-state properties of exotic nuclei. Prog. Part. Nucl. Phys. **57**, 470 (2006). https://doi.org/10.1016/j.ppnp.2005.06.001
22. J. Meng, J.Y. Guo, J. Li et al., Covariant density functional theory in nuclear physics. Progress in Physics **31**, 199–336 (2011)
23. T. Nikšić, D. Vretenar, P. Ring, Relativistic nuclear energy density functionals: mean-field and beyond. Prog. Part. Nucl. Phys **66**, 519 (2011). https://doi.org/10.1016/j.ppnp.2011.01.055
24. J. Meng, Relativistic density functional for nuclear structure, in *International Review of Nuclear Physics*, vol. 10, (World Scientific, Singapore, 2016)
25. J. Meng, P.W. Zhao, *Relativistic Density-Functional Theories* (Springer Nature Singapore, Singapore, 2023), pp.2111–2142
26. T. Nikšić, Z.P. Li, D. Vretenar et al., Beyond the relativistic mean-field approximation. iii. Collective Hamiltonian in five dimensions. Phys. Rev. C **79**, 034303 (2009). https://doi.org/10.1103/PhysRevC.79.034303
27. Z.P. Li, T. Nikšić, D. Vretenar et al., Microscopic analysis of nuclear quantum phase transitions in the $N \approx 90$ region. Phys. Rev. C **79**, 054301 (2009). https://doi.org/10.1103/PhysRevC.79.054301
28. A. Bohr, The coupling of nuclear surface oscillations to the motion of individual nucleons. Mat. Fys. Medd. Dan. Vid. Selsk. **26**, 1 (1952)
29. W. Greiner, J.A. Maruhn, *Nuclear Models* (Spinger-Verlag, Berlin Heidelberg, 1996)
30. L. Próchniak, S.G. Rohoziński, Quadrupole collective states within the Bohr collective Hamiltonian. J. Phys. G Nucl. Part. Phys. **36**, 123101 (2009). https://doi.org/10.1088/0954-3899/36/12/123101
31. K. Matsuyanagi, M. Matsuo, T. Nakatsukasa et al., Open problems in the microscopic theory of large-amplitude collective motion. J. Phys. G Nucl. Part. Phys. **37**, 064018 (2010). https://doi.org/10.1088/0954-3899/37/6/064018
32. T. Nakatsukasa, K. Matsuyanagi, M. Matsuo et al., Time-dependent density-functional description of nuclear dynamics. Rev. Mod. Phys. **88**, 045004 (2016). https://doi.org/10.1103/RevModPhys.88.045004
33. Z.P. Li, T. Nikšić, D. Vretenar, Coexistence of nuclear shapes: selfconsistent mean-field and beyond. J. Phys. G Nucl. Part. Phys. **43**, 024005 (2016). https://doi.org/10.1088/0954-3899/43/2/024005
34. K. Matsuyanagi, M. Matsuo, T. Nakatsukasa et al., Microscopic derivation of the quadrupole collective Hamiltonian for shape coexistence/mixing dynamics. J. Phys. G Nucl. Part. Phys. **43**, 024006 (2016). https://doi.org/10.1088/0954-3899/43/2/024006
35. K. Matsuyanagi, M. Matsuo, T. Nakatsukasa et al., Microscopic derivation of the Bohr-Mottelson collective Hamiltonian and its application to quadrupole shape dynamics. Phys. Scr. **91**, 063014 (2016). https://doi.org/10.1088/0031-8949/91/6/063014
36. Z.P. Li, D. Vretenar, *Model for Collective Motion* (Springer Nature Singapore, Singapore, 2023), pp.1977–2009
37. Z.P. Li, T. Nikšić, D. Vretenar et al., Microscopic analysis of order parameters in nuclear quantum phase transitions. Phys. Rev. C **80**, 061301 (2009). https://doi.org/10.1103/PhysRevC.80.061301
38. Z.P. Li, T. Nikšić, D. Vretenar et al., Microscopic description of spherical to γ-soft shape transitions in ba and xe nuclei. Phys. Rev. C **81**, 034316 (2010). https://doi.org/10.1103/PhysRevC.81.034316
39. Z.P. Li, B.Y. Song, J.M. Yao et al., Simultaneous quadrupole and octupole shape phase transitions in thorium. Phys. Lett. B **726**, 866 (2013). https://doi.org/10.1016/j.physletb.2013.09.035
40. X.Q. Yang, L.J. Wang, J. Xiang et al., Microscopic analysis of prolate-oblate shape phase transition and shape coexistence in the Er-Pt region. Phys. Rev. C **103**, 054321 (2021). https://doi.org/10.1103/PhysRevC.103.054321
41. Z.P. Li, J.M. Yao, D. Vretenar et al., Energy density functional analysis of shape evolution in $N = 28$ isotones. Phys. Rev. C **84**, 054304 (2011). https://doi.org/10.1103/PhysRevC.84.054304
42. K. Nomura, T. Nikšić, T. Otsuka et al., Quadrupole collective dynamics from energy density functionals: collective Hamiltonian and the interacting Boson model. Phys. Rev. C **84**, 014302 (2011). https://doi.org/10.1103/PhysRevC.84.014302
43. H. Mei, J. Xiang, J.M. Yao et al., Rapid structural change in low-lying states of neutron-rich sr and zr isotopes. Phys. Rev. C **85**, 034321 (2012). https://doi.org/10.1103/PhysRevC.85.034321
44. V. Prassa, T. Nikšić, G.A. Lalazissis et al., Relativistic energy density functional description of shape transitions in superheavy nuclei. Phys. Rev. C **86**, 024317 (2012). https://doi.org/10.1103/PhysRevC.86.024317
45. Y. Fu, H. Mei, J. Xiang et al., Beyond relativistic mean-field studies of low-lying states in neutron-deficient krypton isotopes. Phys. Rev. C **87**, 054305 (2013). https://doi.org/10.1103/PhysRevC.87.054305
46. V. Prassa, T. Nikšić, D. Vretenar, Structure of transactinide nuclei with relativistic energy density functionals. Phys. Rev. C **88**, 044324 (2013). https://doi.org/10.1103/PhysRevC.88.044324
47. T. Nikšić, P. Marević, D. Vretenar, Microscopic analysis of shape evolution and triaxiality in germanium isotopes. Phys. Rev. C **89**, 044325 (2014). https://doi.org/10.1103/PhysRevC.89.044325
48. J.M. Yao, K. Hagino, Z.P. Li et al., Microscopic benchmark study of triaxiality in low-lying states of ^{76} Kr. Phys. Rev. C **89**, 054306 (2014). https://doi.org/10.1103/PhysRevC.89.054306
49. J. Xiang, J.M. Yao, Y. Fu et al., Novel triaxial structure in low-lying states of neutron-rich nuclei around $A \approx 100$. Phys. Rev. C **93**, 054324 (2016). https://doi.org/10.1103/PhysRevC.93.054324
50. S. Quan, Q. Chen, Z.P. Li et al., Global analysis of quadrupole shape invariants based on covariant energy density functionals. Phys. Rev. C **95**, 054321 (2017). https://doi.org/10.1103/PhysRevC.95.054321

51. Y. Fu, H. Tong, X.F. Wang et al., Microscopic analysis of shape transition in neutron-deficient yb isotopes. Phys. Rev. C **97**, 014311 (2018). https://doi.org/10.1103/PhysRevC.97.014311
52. Z. Shi, Z.P. Li, Microscopic description of triaxiality in ru isotopes with covariant energy density functional theory. Phys. Rev. C **97**, 034329 (2018). https://doi.org/10.1103/PhysRevC.97.034329
53. J. Xiang, Z.P. Li, W.H. Long et al., Shape evolution and coexistence in neutron-deficient nd and sm nuclei. Phys. Rev. C **98**, 054308 (2018). https://doi.org/10.1103/PhysRevC.98.054308
54. Z. Shi, Q.B. Chen, S.Q. Zhang, Low-lying states in even gd isotopes studied with five-dimensional collective Hamiltonian based on covariant density functional theory. Eur. Phys. J. A **53**, 54 (2018). https://doi.org/10.1140/epja/i2018-12490-9
55. Z. Shi, A.V. Afanasjev, Z.P. Li et al., Superheavy nuclei in a microscopic collective Hamiltonian approach: the impact of beyond-mean-field correlations on ground state and fission properties. Phys. Rev. C **99**, 064316 (2019). https://doi.org/10.1103/PhysRevC.99.064316
56. Y.L. Yang, P.W. Zhao, Z.P. Li, Shape and multiple shape coexistence of nuclei within covariant density functional theory. Phys. Rev. C **107**, 024308 (2023). https://doi.org/10.1103/PhysRevC.107.024308
57. Y.Y. Wang, Z. Shi, Q.B. Chen et al., Tidal wave in ^{102} Pd: an extended five-dimensional collective Hamiltonian description. Phys. Rev. C **93**, 044309 (2016). https://doi.org/10.1103/PhysRevC.93.044309
58. K.Q. Lu, Z.X. Li, Z.P. Li et al., Global study of beyond-mean-field correlation energies in covariant energy density functional theory using a collective Hamiltonian method. Phys. Rev. C **91**, 027304 (2015). https://doi.org/10.1103/PhysRevC.91.027304
59. Y.L. Yang, Y.K. Wang, P.W. Zhao et al., Nuclear landscape in a mapped collective Hamiltonian from covariant density functional theory. Phys. Rev. C **104**, 054312 (2021). https://doi.org/10.1103/PhysRevC.104.054312
60. P.W. Zhao, Z.P. Li, J.M. Yao et al., New parametrization for the nuclear covariant energy density functional with a point-coupling interaction. Phys. Rev. C **82**, 054319 (2010). https://doi.org/10.1103/PhysRevC.82.054319
61. D.J. Thouless, J.G. Valatin, Time-dependent Hartree-Fock equations and rotational states of nuclei. Nucl. Phys. **31**, 211 (1962). https://doi.org/10.1016/0029-5582(62)90741-1
62. J. Libert, M. Girod, J.P. Delaroche, Microscopic descriptions of superdeformed bands with the gogny force: configuration mixing calculations in the $A \sim 190$ mass region. Phys. Rev. C **60**, 054301 (1999). https://doi.org/10.1103/PhysRevC.60.054301
63. N. Hinohara, Z.P. Li, T. Nakatsukasa, T. Nikšić et al., Effect of time-odd mean fields on inertial parameters of the quadrupole collective Hamiltonian. Phys. Rev. C **85**, 024323 (2012). https://doi.org/10.1103/PhysRevC.85.024323
64. Z.P. Li, T. Nikšić, P. Ring et al., Efficient method for computing the thouless-valatin inertia parameters. Phys. Rev. C **86**, 034334 (2012). https://doi.org/10.1103/PhysRevC.86.034334
65. S. Frauendorf, Comment on "stability of the wobbling motion in an odd-mass nucleus and the analysis of ^{135} Pr''. Phys. Rev. C **97**, 069801 (2018). https://doi.org/10.1103/PhysRevC.97.069801
66. Q.B. Chen, S. Frauendorf, Study of wobbling modes by means of spin coherent state maps. Eur. Phys. J. A **58**, 75 (2022). https://doi.org/10.1140/epja/s10050-022-00727-5
67. J. Meng, S.Q. Zhang, Open problems in understanding the nuclear chirality. J. Phys. G Nucl. Part. Phys. **37**, 064025 (2010). https://doi.org/10.1088/0954-3899/37/6/064025
68. J. Meng, Q.B. Chen, S.Q. Zhang, Chirality in atomic nuclei: 2013. Int. J. Mod. Phys. E **23**, 1430016 (2014). https://doi.org/10.1142/S0218301314300161
69. J. Meng, P.W. Zhao, Nuclear chiral and magnetic rotation in covariant density functional theory. Phys. Scr. **91**, 053008 (2016). https://doi.org/10.1088/0031-8949/91/5/053008
70. Q.B. Chen, J. Meng, Novel excitation modes in nuclei: experimental and theoretical investigation on multiple chiral doublets. Nucl. Phys. News **30**, 11 (2020). https://doi.org/10.1080/10619127.2019.1676119
71. See: http://www.nndc.bnl.gov/ensdf/
72. W. Zhang, W. Gao, G.T. Zhang et al., Level density of odd-A nuclei at saddle point. Nucl. Sci. Tech. **34**, 124 (2023). https://doi.org/10.1007/s41365-023-01270-8
73. K.P. Geng, P.X. Du, J. Li et al., Calculation of microscopic nuclear level densities based on covariant density functional theory. Nucl. Sci. Tech. **34**, 141 (2023). https://doi.org/10.1007/s41365-023-01298-w
74. X. Guan, J.H. Zhang, M.Y. Zheng, Pairing effects on the fragment mass distribution of th, u, pu, and cm isotopes. Nucl. Sci. Tech. **34**, 173 (2023). https://doi.org/10.1007/s41365-023-01316-x
75. Y.F. Gao, B.S. Cai, C.X. Yuan, Investigation of β^--decay half-life and delayed neutron emission with uncertainty analysis. Nucl. Sci. Tech. **34**, 9 (2023). https://doi.org/10.1007/s41365-022-01153-4
76. J. Xiang, Z.P. Li, T. Nikšić et al., Coupling shape and pairing vibrations in a collective hamiltonian based on nuclear energy density functionals (ii): low-energy excitation spectra of triaxial nuclei. arXiv: nucl-th, 2312.01791 (2023). https://doi.org/10.48550/arXiv.2312.01791
77. N.V. Zamfir, R.F. Casten, Signatures of γ softness or triaxiality in low energy nuclear spectra. Phys. Lett. B **260**, 265 (1991). https://doi.org/10.1016/0370-2693(91)91610-8
78. J. Xiang, Z.P. Li, T. Nikšić et al., Coupling of shape and pairing vibrations in a collective Hamiltonian based on nuclear energy density functionals. ii. low-energy excitation spectra of triaxial nuclei. Phys. Rev. C **109**, 044319 (2024). https://doi.org/10.1103/PhysRevC.109.044319
79. G. Coló, A novel way to study the nuclear collective excitations. Nucl. Sci. Tech. **34**, 189 (2023). https://doi.org/10.1007/s41365-023-01343-8
80. X.X. Sun, S.G. Zhou, Deformed halo nuclei and shape decoupling effects. Nucl. Tech. (in Chinese) **46**, 080015 (2023). https://doi.org/10.11889/j.0253-3219.2023.hjs.46.080015
81. S. Zhang, Y.F. Geng, F.R. Xu, Ab initio Gamow shell-model calculations for dripline nuclei. Nucl. Tech. (in Chinese) **46**, 080012 (2023). https://doi.org/10.11889/j.0253-3219.2023.hjs.46.080012
82. Y. Chen, Y.L. Ye, K. Wei, Progress and perspective of the research on exotic structures of unstable nuclei. Nucl. Tech. (in Chinese) **46**, 080020 (2023). https://doi.org/10.11889/j.0253-3219.2023.hjs.46.080020